대한기계학회 2000년도 추계학술대회논문집 A pp. 387~394 KSME 00F050

CONTACT PRESSURE DISTRIBUTION OF RADIAL TIRE IN MOTION WITH CAMBER ANGLE

Seoknam KIM * · Kyohei KONDO ** · Takashi AKASAKA***

KEY WORDS : Camber angle, radial tire in motion, trapezoidal contact patch, stepwise analysis, nonlinear sidewall spring constant, contact pressure distribution

ABSTRACT

Theoretical and experimental study is conducted on the contact pressure distribution of a radial tire in motion under various camber angles. Tire construction is modelled by a spring bedded elastic ring, consisted of sidewall springs and a composite belt ring. The contact area is assumed to be a trapezoidal shape varying with camber angles and weighted load. The basic equation in a quasi-static form is derived for the deformation of a running belt with a constant velocity by the aid of Lagrange-Euler transformation. Galerkin's method and stepwise calculation are applied for solving the basic equation and the mechanical boundary condition along both sides of the contact belt part subjected to shearing forces transmitted from the sidewall spring.

Experimental results on the contact pressure, measured by pressure sensors embedded in the surface of the drum tester, correspond well with the calculated ones for the test tire under various camber angles, running velocities and weighted loads.

These results indicate that a buckling phenomenon of the contact belt in the widthwise direction occurs due to the effect of camber angle.

1 Introduction

Analysis on the contact deformation to the roadway and the contact pressure distribution of a radial tire in motion with camber angle has been an important problem deeply related to the cornering characteristics and the abrasion properties of tire. This analytical study is evident to conflict with the mathematical difficulties attributed to large deformation and nonlinear properties of the tire contacting obliquely to the roadway and therefore it has not yet been conducted satisfactorily.

Recently, Kagami et al[2] analyzed the contact deformation of a radial tire with camber angles under the static load in the vertical direction. Utilizing the Böhms[1] theory for the contact-free part of the belt, they solved approximately the two dimensional deformation of the contact belt by the use of Galerkin's method.

On the other hand, Shiobara et al[3] presented a research paper on the contact deformation of a radial tire in motion without camber angle. This lead to a clear understanding for the contact pressure rise at the leading edge of the contact area of a rotating radial tire, however did not consider also the non-linear property of sidewall springs.

Then, we intend here to determine the contact pressure distribution of a radial tire in motion with camber angles by extending and revising these two papers mentioned above.

Introducing a new method of stepwise analysis taken the nonlinearity of a sidewall spring into consideration, and also simplifying the expressions for membrane forces in the contact belt, we endeavored to obtain the contact pressure distribution without so much numerical calculations. We conducted further an experimental study of the contact pressure distribution under various camber angles and running velocities to verify predicted results.

* R & D Center, Hankook Tire Co., LTD, 23-1 Jang Dong, Yusung-Gu, Taejon 305-343, KOREA

** Department of Aeronautics and Astronautics Engineering,The University of Tokyo, 7-3-1 Honggo, Bunkyo-ku, Tokyo 113, JAPAN

*** Chuo University,742-1 Higashi-Nakano, Hachiohji-shi, Tokyo 192-03,JAPAN

2 Contact-Free Belt

We denote the coordinate axes of the belt ring in the widthwise, the circumferential and the inward normal directions by x,y and z, and displacement by u,v and w respectively, and further the twist angle around y axis by $\phi(y)$, as shown in Fig.1, where θ_0 signifies a half central angle contained by the arc length of the contact belt part.

An element of the belt ring is supported by side-wall spring systems in the radial, lateral and tangential directions of which spring constants are denoted by K_r, K_s and K_t respectively,[4].

Considering that the belt element is subjected to the inflation pressure p, the extensional force in the y direction $\overline{N}_y$, due to the torque T, the in-plane bending moment M_z, the out-of-plane bending moment M_x, transverse shearing force F, and inertia forces a_x, a_y and a_z shown in Fig.2 and assuming that the belt ring is in-extensible, we obtain the following equilibrium equations for the steady state case.

i) Equilibrium condition in z direction yields

$$v^{(6)} + \alpha_1 v^{(4)} + \alpha_2 v^{(2)} + \alpha_3 v = 0 \tag{1}$$

$$w = v' \tag{2}$$

where prime($'$) implies the differentiation with respect to θ and the coefficients are given by

$$\begin{aligned} \alpha_1 &= 2 - \frac{\overline{N}_y a^2 b}{D_x} + \frac{\rho a^4 b \Omega^2}{D_x} \\ \alpha_2 &= 1 + \frac{\overline{K}_r a^4}{D_x} - \frac{\overline{N}_y a^2 b}{D_x} - \frac{6\rho a^4 b \Omega^2}{D_x} \\ \alpha_3 &= \frac{\rho a^4 b \Omega^2}{D_x} - \frac{K_t a^4}{D_x} \end{aligned} \tag{3}$$

where D_x denotes the out-of-plane bending stiffness of the belt, and Eq(2) means the in-extensibility condition of the belt.

ii) Equilibrium condition in x direction yields

$$u^{(4)} + \delta_1 u^{(2)} + \delta_2 u + \delta_3 \phi^{(2)} + \delta_4 \phi = 0 \tag{4}$$

$$\begin{aligned} \delta_1 &= -\frac{\overline{N}_y a^2}{D_z} - \frac{\Gamma}{D_z} + \frac{\rho a^4 b \Omega^2}{D_z} \\ \delta_2 &= \frac{K_s a^4}{D_z} \\ \delta_3 &= a + \frac{a\Gamma}{D_z} \\ \delta_4 &= -\frac{\rho a^4 b}{D_z} \end{aligned} \tag{5}$$

and further D_z and Γ signify the in-plane bending and the torsional stiffness respectively.

iii) Equilibrium condition in y direction yields

$$u'' + \gamma_1 \phi'' + \gamma_2 \phi = 0 \tag{6}$$

$$\begin{aligned} \gamma_1 &= \frac{(\Gamma - Ia^2\Omega^2)a}{\Gamma + D_z} \\ \gamma_2 &= \frac{(D_z + \overline{K}_r a^2 b^2/4)a}{\Gamma + D_z} \end{aligned} \tag{7}$$

and I denotes the moment of inertia for the unit length of the belt.

In deriving these equilibrium equations, we used the Lagrange-Euler trasformations as

$$\frac{\partial^2}{\partial t^2} = \Omega^2 \frac{\partial^2}{\partial \theta^2} \tag{8}$$

for the steady state deformation

3 Difference Equations and Boundary Conditions

Since the radial spring constant K_r has a tendency of steep decent as the increase of inward deflection as well known[4], then we intend to conduct a stepwise analysis[5] for displacement functions of u, v, w and ϕ. Then, we transform the differential equations of Eqs(1), (4) and (6) to finite difference equations.

Eq(1) is transformed to the following difference equation, in j-th loading case.

$$v_{i+3} + \beta_1 v_{i+2} + \beta_2 v_{i+1} + \beta_3 v_i + \beta_4 v_{i-1} + \beta_5 v_{i-2} + v_{i-3} = 0 \tag{9}$$

where superscript j is omitted, and the coefficents are listed below.

$$\begin{aligned} \beta_1 &= -6 + \alpha_1 \Delta\theta^2 \\ \beta_2 &= 15 - 4\alpha_1 \Delta\theta^2 + \alpha_{2i} \Delta\theta^4 \\ \beta_3 &= -20 + 6\alpha_1 \Delta\theta^2 - 2\alpha_{2i} \Delta\theta^4 + \alpha_3 \Delta\theta^6 \\ \beta_4 &= 15 - 4\alpha_1 \Delta\theta^2 + \alpha_{2i} \Delta\theta^4 \\ \beta_5 &= -6 + \alpha_1 \Delta\theta^2 \end{aligned} \tag{10}$$

Boundary conditions for this difference equation are described below.

(a) Symmetry condition at the apex :

$$v_{n+1} - 2v_n + v_{n-1} = 0 \tag{11}$$

(b)Tangential rotation at the contact belt end :

$$v_{j+1} + (-2 + \Delta\theta^2) v_j + v_{j-1} = -ja\Delta\theta^3 \tag{12}$$

(c) Out-of-plane bending moment at the contact belt end :

$$v_{j+2}-(2-\Delta\theta^2)v_{j+1}+(2-\Delta\theta^2)v_{j-1}-v_{j-2}=0 \quad (13)$$

(d) Horizontal displacement at the contact belt end :

$$-v_{j+1}\sin(j\Delta\theta)+2\Delta\theta v_j\cos(j\Delta\theta)+v_{j-1}\sin(j\Delta\theta)=\frac{a}{3}j^3\Delta\theta^4 \quad (14)$$

Eqs(4) and (6) are replaced by the following difference equations respectively

$$u_{i+2}+\nu_1 u_{i+1}+\nu_2 u_i+\nu_1 u_{i-1}+u_{i-2}+\lambda_1\phi_{i+1}+\lambda_2\phi_i+\lambda_1\phi_{i-1}=0 \quad (15)$$

$$u_{i+1}-2u_i+u_{i-1}+\gamma_1\phi_{i+1}+\bar{\gamma}_{1i}\phi_i+\gamma_1\phi_{i-1}=0 \quad (16)$$

where

$$\begin{aligned}\nu_1 &= \delta_1\Delta\theta^2-4\\ \nu_2 &= 6-2\delta_1\Delta\theta^2+\delta_2\Delta\theta^4\\ \lambda_1 &= \delta_3\Delta\theta^2\\ \lambda_2 &= \delta_4\Delta\theta^4-2\delta_3\Delta\theta^2\\ \bar{\gamma}_1 &= \gamma_2\Delta\theta^2-2\gamma_1\end{aligned} \quad (17)$$

Boundary conditions for this difference equation system are described as follows.

(a') Symmetry conditions at the apex :

$$u_{n+1}=u_{n-1}\ , \quad u_{n+2}=u_{n-2} \quad (18)$$

$$\phi_{n+1}=\phi_{n-1}\ , \quad \phi_{n+2}=\phi_{n-2} \quad (19)$$

however, it is noted that $u_n\neq 0$ and $\phi_n u_n\neq 0$.

(b') Torsional angle at the contact belt end :

$$\phi_j=-\alpha \quad (20)$$

(c') Lateral displacement at the contact belt end :

$$u_j=(Z_j+\zeta_j)\tan\alpha \quad (21)$$

(d') In-plane shearing force at the contact end :

$$D_z\left\{\frac{u_{j+2}-2u_{j+1}+2u_{j-1}-u_{j-2}}{2a^3\Delta\theta^3}+\frac{\phi_{j+1}+\phi_{j-1}}{2a^2\Delta\theta}\right\}$$
$$+\Gamma\left\{\frac{\phi_{j+1}-\phi_{j-1}}{2a^2\Delta\theta}-\frac{u_{j+1}-u_{j-1}}{2a^3\Delta\theta}\right\}=K_s a\Delta\theta\sum_{i=j}^{n}u_i \quad (22)$$

The in-plane bending moment M_z, and the torsional moment T, at $\theta=\theta_0$ are obtained as

$$M_{z,j}=\frac{D_z\gamma_1}{a^2\Delta\theta^2}\left[\phi_{j+1}+\left\{-2+\frac{1}{\gamma_1}\Delta\theta^2(\gamma_2-a)\right\}\phi_j+\phi_{j-1}\right] \quad (23)$$

$$T_j=\frac{\Gamma}{2a\Delta\theta}\left\{\phi_{j+1}-\phi_{j-1}-\frac{1}{a}(u_{j+1}-u_{j-1})\right\} \quad (24)$$

4 Contact Deformation and Contact Shear

The contact area of the belt behaves like a quasi-trapezoidal shape slightly bent in the camber direction as illustrated in Fig.3.

The taper angle β of the trapezoidal contact area becomes

$$\tan\beta=\frac{\overline{p}_1'\overline{r}_1'-\overline{p}_2'\overline{s}_2'}{b}\simeq\frac{\overline{a}(\overline{\theta}_1-\overline{\theta}_2)}{b} \quad (25)$$

Otherwisely

$$\tan\alpha\simeq\frac{\overline{a}}{2b}(\overline{\theta}_1^2-\overline{\theta}_2^2)=\tan\beta\frac{\overline{\theta}_1+\overline{\theta}_2}{2} \quad (26)$$

Then, we have

$$\beta=\tan^{-1}\left(\frac{\tan\alpha}{\theta_0}\right)\ , \quad \left(\theta_0\equiv\frac{\overline{\theta}_1+\overline{\theta}_2}{2}\right) \quad (27)$$

where θ_0 implies a half central angle at the contact end along the middle line of the belt.

The total deflection δ, in the vertical direction(Z) is represented by

$$\delta\simeq(Z_1+\overline{\zeta_1})\cos\alpha=\left\{a(1-\cos\overline{\theta}_1)+\overline{\zeta_1}\right\}\cos\alpha \quad (28)$$

where Z_1 denotes the geometrical height in the vertical (Z) direction at the contact end of the front belt periphery, while $\overline{\zeta_1}$ denotes the elastic displacement in Z direction referred to [5].

Kagami et al[2] assumed that the in-plane shapes of the deformed belt and the tread rubber surface to be both slightly bent trapezoids as illustrated in Fig.4 and derived the following representations for the maximum relative movement, A, and the curvature of the front side of the contact belt $1/R_1$.

$$A=\frac{a}{4}\frac{\sin^4\theta_1}{\cos\theta_1}\sin\alpha\cos\alpha \quad (29)$$

$$\frac{1}{R_1}=\frac{\sin\alpha}{a}\left(1-\frac{1}{2}\frac{\sin^2\theta_1}{\cos\theta_1}\cos\alpha\right)\simeq\frac{\sin\alpha}{a} \quad (30)$$

Noting that the relative movement between these quasi-trapezoids vanishes along the common oblique sides, we can represent the relative movement, ΔU, as

$$\Delta U=A\left(1-\frac{y^2}{\overline{y}^2}\right) \quad (31)$$

where $\overline{y}(x)$ is a geometrical function for a straight oblique side of the quasi-trapezoid as

$$\overline{y}(x) = \frac{\overline{y}_1 + \overline{y}_2}{2} + \frac{\overline{y}_2 - \overline{y}_1}{b} x \quad (\overline{y}_1 = a \sin\theta_1,\ \overline{y}_2 = a \sin\theta_2) \tag{32}$$

Then, the contact shear, S_x, is given by

$$S_x = \frac{G}{H} A \left(1 - \frac{y^2}{\overline{y}^2}\right) \tag{33}$$

where H is the thickness of tread rubber.

The contact shear in the circumferential direction of y, S_y, is inherent to the bending deformation and simply represented as

$$S_y = G\theta \tag{34}$$

Then, the camber thrust, Q_x, can be given by

$$\begin{aligned} Q_x &= 2\frac{GA}{H} \int_{-\frac{b}{2}}^{\frac{b}{2}} \int_0^{\overline{y}(x)} \left\{1 - \frac{y^2}{\overline{y}^2(x)}\right\} dy\, dx \\ &= \frac{G}{12H} a^2 b \frac{\sin^4\theta_1}{\cos\theta_1} (\sin\overline{\theta}_1 + \sin\overline{\theta}_2) \sin 2\alpha \end{aligned} \tag{35}$$

5 Membrane Forces in the Contact Belt

Initially the whole belt has been subjected to the following initial membrane forces, $\overline{N}_x$ and $\overline{N}_y$, in the widthwise and the circumferential directions respectively, due to the inflation pressure p

$$\overline{N}_x = \frac{p({r_D}^2 - {r_C}^2)}{2r_D} \tag{36}$$

$$\overline{N}_y = pr_D \left(1 - \frac{({r_D}^2 - {r_C}^2)}{r_D b} \cot\phi_D\right) \tag{37}$$

where r_C, r_D are radius coordinates of the turning point, C, and the sidewall end, D, respectively and ϕ_D denotes the tangential angle at D of a tire cross section(cf. Fig.1).

We intend here to obtain membrane forces, N_x, N_y and N_{xy} of the contact belt in the contact state, as shown in Fig.5.

For simplicity, neglecting the additional terms *transmitted from the contact-free belt, we assume* here as

$$N_x = \overline{N}_x \tag{38}$$

$$N_y = \overline{N}_y + N_B x \tag{39}$$

where $N_B x$ signifies the bending membrane force, with the notation of

$$N_B = \frac{hE_y}{R_0} \tag{40}$$

In the above representations, h is the thickness of the belt, E_y is the orthotropic modulus in y direction and R_0 is the in-plane radius of curvature of the bent belt, which are represented by

$$E_y = E_m \left(1 - \cot^2\alpha_0 + \cot^4\alpha_0\right) \tag{41}$$

$$\frac{1}{R_0} = \frac{\sin\alpha}{a} \tag{42}$$

where E_m implies modulus of rubber and α_0 denotes bias angle of the composite belt.

Shearing membrane force, N_{xy}, can be obtained from the equilibrium equation and Eq(33)

$$\frac{\partial N_x}{\partial x} + \frac{\partial N_{xy}}{\partial y} = -S_x \tag{43}$$

as follows

$$\begin{aligned} N_{xy} &= -\int_{-\overline{y}}^{\overline{y}} S_x\, dy \\ &= -\frac{GA}{H}\left(y - \frac{y^3}{3\overline{y}^2}\right) \end{aligned} \tag{44}$$

which satisfies the condition of $N_{xy} = 0$ along $y = 0$.

6 Deflection of Contact Belt

We establish first the standard flat deflection surface, $w_0(x, y)$, which is inclined slightly to the roadway plane in the front side direction of the contact trapezoid, and then consider an additional deflection, $\overline{w}(x, y)$, which is to be superimposed upon $w_0(x, y)$.

We can put

$$w_0(x, y) = -\omega_1 - \omega_2 x \tag{45}$$

where ω_1 implies a uniform deflection, while ω_2 means a rotation angle around y axis.

The total deflection $w^*(x, y)$ is thus represented by

$$w^*(x, y) = w_0(x, y) + \overline{w}(x, y) \tag{46}$$

Referring to Fig.6, we have the following equilibrium equation for $\overline{w}(x,y)$

$$D_{xx}\overline{w}_{,xxxx} + 2(D_{xy}+2D_{ss})\overline{w}_{,xxyy} + D_{yy}\overline{w}_{,yyyy} = -p - \rho V^2\overline{w}_{,yy} + q + \overline{N}_x\overline{w}_{,xx} + N_y\overline{w}_{,yy} + 2N_{xy}\overline{w}_{,xy} \quad (47)$$

where D_{xx}, D_{yy}, D_{xy} and D_{ss} are bending and torsional stiffnesses of an orthotropic plate corresponding to the composite belt structure, V signifies the velocity of contact belt in motion, and q denotes the contact pressure represented by

$$q(x,y) = -K_m w^*(x,y) + C_m V\overline{w}_{,y} \quad (48)$$

with the use of spring constant, K_m, and visco-elastic coefficient, C_m, of the tread rubber, together with Lagrange-Euler transformation.

The boundary conditions for tranverse shearing force, Q_{x1}, along x=-b/2 and Q_{x2} along x=b/2 are given respectively by

at $x = -b/2$

$$(D_{xy}+2D_{ss})\overline{w}_{1,xyy} + D_{xx}\overline{w}_{1,xxx} = -\frac{1}{2}\overline{K}_r(\xi_1)\xi_1 \quad (49)$$

at $x = b/2$

$$(D_{xy}+2D_{ss})\overline{w}_{2,xyy} + D_{xx}\overline{w}_{2,xxx} = \frac{1}{2}\overline{K}_r(\xi_2)\xi_2 \quad (50)$$

where ξ_1 and ξ_2 denote the deflections of sidewall spring along x=-b/2 and x=b/2 respectively, represented as

$$\xi_1(y) = Z_1 - Z + \overline{\zeta}_1 + \overline{w}_1\cos\alpha \simeq \frac{1}{2a}(\overline{y}_1^2 - y^2) + \overline{\zeta}_1 \quad (51)$$

$$\xi_2(y) = Z_2 - Z + \overline{\zeta}_2 + \overline{w}_2\cos\alpha \simeq \frac{1}{2a}(\overline{y}_2^2 - y^2) + \overline{\zeta}_2 \quad (52)$$

by neglecting the terms of $\overline{w}_i\cos\alpha (i=1,2)$, and refferring to Fig.6, $\overline{y}_1$ and $\overline{y}_2$ are given by

$$\begin{aligned} \overline{y}_1 &= c + \frac{b}{2}\tan\beta \\ \overline{y}_2 &= c - \frac{b}{2}\tan\beta, \quad (c = a\theta_0) \end{aligned} \quad (53)$$

The boundary conditions for out-of-plane bending moment M_{x1} along $x = -b/2$ and M_{x2} along $x = b/2$, being both assumed to vanish, are given respectively by

at $x = -b/2$

$$D_{xx}\overline{w}_{1,xx} + D_{xy}\overline{w}_{1,yy} = 0 \quad (54)$$

at $x = b/2$

$$D_{xx}\overline{w}_{2,xx} + D_{xy}\overline{w}_{2,yy} = 0 \quad (55)$$

7 Determination of ω_1 and ω_2

Quantities of ω_1 and ω_2 given in Eq(45), predicting the standard plane of deflection, are determined from the equilibrium conditions concerning the vertical load W and the torsional moment T around y axis at the contact end(cf. Fig.7).

The vertical load W is described in two ways. as

$$W = \int_{-b/2}^{b/2}\int_{-\overline{y}}^{\overline{y}} q\,dx\,dy = K_m\int_{-b/2}^{b/2}\int_{-\overline{y}}^{\overline{y}}(\omega_1 + \omega_2 x - \overline{w})\,dx\,dy \quad (56)$$

and

$$\begin{aligned} W &= 2pbc + 2F + \rho V^2\int_{-\overline{y}^j}^{\overline{y}^j}\int_{-b/2}^{b/2}\overline{w}_{,yy}\,dx\,dy \\ &\quad + \frac{1}{2}\int_{-\overline{y}_1^j}^{\overline{y}_1^j}\overline{K}_{r1}\xi_1\,dy + \frac{1}{2}\int_{-\overline{y}_2^j}^{\overline{y}_2^j}\overline{K}_{r2}\xi_2\,dy \end{aligned} \quad (57)$$

where Eqs(56) and (57) mean the downward and the upward total load W.

By neglecting $\overline{w}$ in the first integral of Eq(56), because of being small compared with ω_1 and seeing that the second integral vanishes when $\overline{w}(x,y)$ is symmetric with respect to y, we have

$$W \approx K_m\left(2\omega_1 bc - \frac{1}{6}\omega_2 b^3\tan\beta\right) \quad (58)$$

Then, neglecting the third term integral on the right-hand side of Eq(57), we have

$$\begin{aligned} W &\approx 2pbc + 2F + \overline{K}_{r1}(\xi_1)\left(\frac{(\overline{y}_1)^3}{3a} + 2\overline{\zeta}_1\overline{y}_1\right) \\ &\quad + \overline{K}_{r2}(\xi_2)\left(\frac{(\overline{y}_2)^3}{3a} + 2\overline{\zeta}_2\overline{y}_2\right) \end{aligned} \quad (59)$$

Elimination W from Eqs(58) and (59) gives an equation for ω_1 and ω_2.

Eq(59) is used to calculate the vertical load , W, in the j-th step.

As shown in Fig.7, equilibrium condition for the torsional moment around y axis attributed to the inflation pressure, p, reaction forces from the sidewall spring and the tread rubber spring and torque T transmitted from the contact-free belt, which is given by Eq(24), is represented as

$$\begin{aligned} &T + \frac{b}{2}\cos\alpha\left\{\int_{-\overline{y}}^{\overline{y}}\overline{K}_r(\xi_1)\,dy - \int_{-\overline{y}}^{\overline{y}}\overline{K}_r(\xi_2)\,dy\right\} \\ &+K_m\int_{-\overline{y}}^{\overline{y}}\int_{-b/2}^{b/2}xw_0\,dx\,dy - p\int_{-\overline{y}}^{\overline{y}}\int_{-b/2}^{b/2}x\,dx\,dy = 0 \end{aligned} \quad (60)$$

which provides another equation for ω_1 and ω_2.

8 Galerkin's Method

Additional deflection $\overline{w}(x,y)$, included in the fundamental Eq(47), could be given by

$$\overline{w}(x,y) = f(x)(\overline{y}(x)^2 - y^2)^2 \tag{61}$$

which satisfies the boundary conditions(clamped supported) along the oblique lines of the contact patch, $y = \pm\overline{y}(x)$:

$$\overline{w} = 0, \qquad \overline{w}_y = 0 \tag{62}$$

where $f(x)$ put fifth polynominal to x, as

$$f(x) = a_0 + a_1 x + a_2 x^2 + a_3 x^3 + a_4 x^4 + a_5 x^5 \tag{63}$$

Considering Eqs(38), (39) and (44), together with Eq (48), we can rewrite Eq(47) as follows

$$\begin{aligned} &D_{xx}\overline{w}_{,xxxx} + 2(D_{xy} + 2D_{ss})\overline{w}_{,xxyy} + D_{yy}\overline{w}_{,yyyy} \\ &= -p + K_m(\overline{N}_y - \rho V^2 + N_B x)\overline{w}_{,yy} + C_m V \overline{w}_{,y} \\ &+\overline{N}_x \overline{w}_{,xx} + 2N_{xy}\overline{w}_{,xy} \end{aligned} \tag{64}$$

In order to determine six constants of a_0, a_1, a_2, a_3, a_4 and a_5 including in Eq(63) as satisfying Eq(64) and four boundary conditions of Eqs(49), (50), (54) and (55), it is convenient to use the Galerkin's method.

Then, two weight functions of $\rho_1(x,y)$ and $\rho_2(x,y)$ described below are adopted for this purpose.

$$\rho_1(x,y) = (\overline{y}(x)^2 - y^2)^2 \tag{65}$$

$$\rho_2(x,y) = x(\overline{y}(x)^2 - y^2)^2 \tag{66}$$

Applying the weight function of $\rho_1(x,y)$ and $\rho_2(x,y)$ for Eq(64) and $\rho_1(x,y)$ for four boundary conditions Eqs(50), (51), (54) and (55) respectively, we have the following six equations.

$$\int_{-b/2}^{b/2}\int_{-\overline{y}}^{\overline{y}} e(x,y)\rho_1(x,y)\,dy\,dx = 0 \tag{67}$$

$$\int_{-b/2}^{b/2}\int_{-\overline{y}}^{\overline{y}} e(x,y)\rho_2(x,y)\,dy\,dx = 0 \tag{68}$$

$$\int_{-\overline{y}_i}^{\overline{y}_i} \overline{e}_{1i}(x,y)\rho_1(x,y)\,dy = 0, \ (i = 1,2) \tag{69}$$

$$\int_{-\overline{y}_i}^{\overline{y}_i} \overline{e}_{2i}(x,y)\rho_1(x,y)\,dy = 0, \ (i = 1,2) \tag{70}$$

where

$$\begin{aligned} e(x,y) &= D_{xx}\overline{w}_{,xxxx} + 2(D_{xy} + 2D_{ss})\overline{w}_{,xxyy} + D_{yy}\overline{w}_{,yyyy} \\ &+p + \rho V^2 \overline{w}_{,yy} - q - N_x \overline{w}_{,xx} - N_y \overline{w}_{,yy} - 2N_{xy}\overline{w}_{,xy} \end{aligned} \tag{71}$$

$$\begin{aligned} \overline{e}_{1i} &= (D_{xy} + 2D_{ss})\overline{w}_{i,xyy} + D_{xx}\overline{w}_{i,xxx} \\ &+\frac{1}{2}\overline{K}_r(\xi_i)\left\{\frac{1}{2a}\left((\overline{y}_i)^2 - (y)^2\right) + \zeta_i\right\}\cos\alpha \end{aligned} \tag{72}$$

$$\overline{e}_{2i} = D_{xx}\overline{w}_{i,xx} + D_{xy}\overline{w}_{i,yy} \tag{73}$$

9 Comparision of Calculated and Experimental Results

Experimental study was conducted to verify the calculated results for the same passenger radial tire, 175SR14, as that adopted as the numerical example.

Fig.8 gives the relationship between vertical load and the deflection of the front side. we cann't use that's relationship when load is small, because two side shoulders don't touched on roadway by camber angle.

Fig.9 shows the distribution of circumferential membrane force N_y in the contact belt, under the vertical load $W = 4KN$, camber angle $\alpha = 1°$ and velocity $V = 0km/h$.

Membrane force N_y in the circumferential direction happens to be compressive along the front side of the contact belt, attributed to its in-plane bending deformation of the belt with camber angle α.

Figures.10, 11 illustrate the contact pressure distribution in the circumferential direction, at x=-15, -41.5mm apart from the crown center in the front direction, when p=0.18MPa, W=4KN, V=10,60km/h and $\alpha = 2°$.

As shown in Figures.10, 11, the partial floating-up phenomenon of the contact belt ,causing the contact pressure to be zero, might take place due to camber angle without the velocity and at the crown center parts in the front side direction.

10 Conclusion

we obtained the following concluding remarks.

1. Spring effect of the whole tire in the vertical direction increases slightly with the increase the running velocity, V, and decreases with the increase of camber angle, α.

2. Camber thrust Q_x increases steeply with the increase of the vertical load W, and increases linearly with the increase of the camber angle, α, while it increases slightly with the increase of the velocity, V.

3. Contact pressure distribution behaves like a deep concave along the crown center, and like a shallow convex curve both along front and rear sides of the trapezoidal contact area.

   The predicted distributions of the contact pressure are verified by the experimental results.

4. It is obserbed that the contact pressure rises more along the trailing edge than along the leading edge due to the viscosity effect in high temperature.

5. Membrane force N_y in the circumferential direction happens to be compressive along the front side of the contact belt, attributed to its in-plane bending deformation of the belt with camber angle.

6. The partial floating-up phenomenon of the contact belt might take place, causing the contact pressure to be zero, when the camber angle grows to some extent.

References

[1] Böhm F., ATZ,Bd.69,Nr.8,1969,WT.255-261.

[2] Kagami S., Akasaka T., Shiobara H. and Hasegawa A., TSTCA,vol.23,No.1,1995, pp.26-51.

[3] Kagami S., Akasaka T., Shiobara H. and Hasegawa A., TSTCA,vol.24,No.4,1996, pp.294-320.

[4] Kim S., Kondo K. and Akasaka T.,Journal of Soc. Rubber Ind.,Japan,vol.70,No.7,1997,pp.409-414.

[5] Kim S., Kondo K. and Akasaka T., Journal of Soc. Rubber Ind.,Japan, vol.71,No.1,1998,pp.33-40.

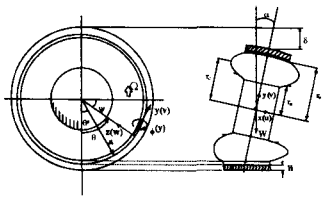

Fig.1 Coordinate axes of x,y and z,and displacement of u,v and w established along the belt

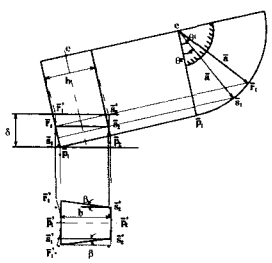

Fig.3 The oblique side of $\bar{F}_i\bar{R}_i$ of a trapezoidal contact patch

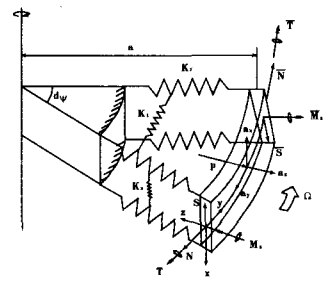

Fig.2 Forces and moments applied to an element of the contact-free belt

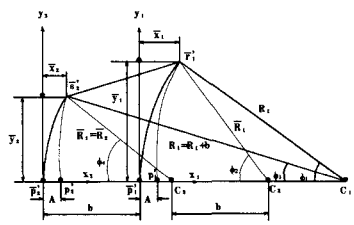

Fig.4 In-plane bending deformation of the contact belt

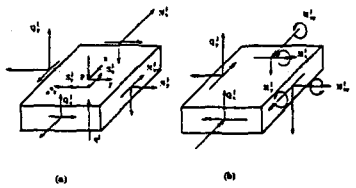

Fig.5 Membrane forces, transverse shearing forces, moments, inflation pressure, contact pressure and inertia forces of belt element in the contact region

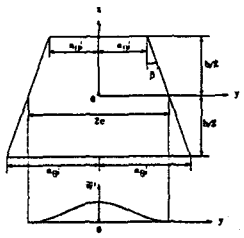

Fig.6 Trapezoidal contact patch and the additional deflection, $\bar{w}'$

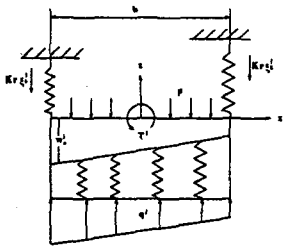

Fig.7 Moment equilibrium around y axis of the contact belt

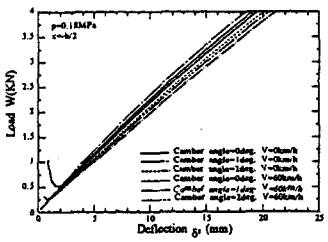

Fig.8 Relationship between load and deflection d1 in the front side, when p=0.18MPa, V=0,60km/h and camber angle=0,1,2deg.

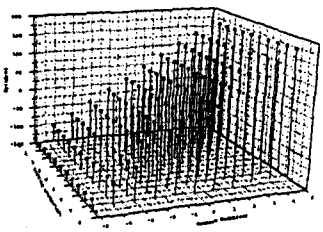

Fig.9 3-D distribution of membrane force Ny in the circumferential direction, when p=0.18MPa, W=4KN, V=0km/h and camber angle=1deg.

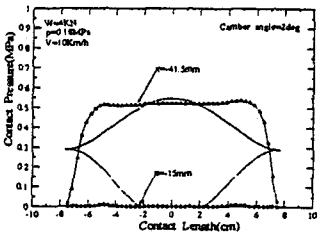

Fig.10 Contact pressure distribution in the circumferential direction at x=-15,41.5mm apart from the crown center in the front side, when p=0.18MPa, W=4KN, V=10km/h and camber angle=2deg.

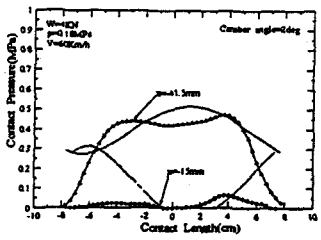

Fig.11 Contact pressure distribution in the circumferential direction at x=-15,-41.5mm apart from the crown center in the front side when p=0.18MPa, W=4KN, V=60km/h and camber angle=2deg.